JOURNAL OF MODERN OPTICS, 2003, VOL. 50, NO. 10, 1615–1625

Behaviour of an optically trapped probe approaching a dielectric interface

PETR JÁKL[†], MOJMÍR ŠERÝ[†‡], JAN JEŽEK[†], ALEXANDR JONÁŠ[†], MIROSLAV LIŠKA[‡] and PAVEL ZEMÁNEK[†]

[†]Institute of Scientific Instruments, Academy of Sciences of the Czech Republic, Brno, Czech Republic; e-mail: jakl@isibrno.cz; http://www.isibrno.cz
[‡]Institute of Physical Engineering, Brno University of Technology, Brno, Czech Republic
email: jakl@isibrno.cz

(*Received 12 September 2002; revision received 11 November 2002*)

Abstract. The way in which reflection of the trapping beam from a dielectric interface influences the distance of the trapped sphere from the beam waist is studied theoretically and experimentally. The reflected wave interferes with the incident wave and they create a standing-wave component in the total axial intensity distribution. This component then modulates the trapping potential and creates several possible equilibrium positions for the trapped sphere. When the beam waist approaches the surface, the potential profile changes, which consequently causes jumps of the trapped probe from its current location to a deeper potential well. We suggested theoretically and proved experimentally that the magnitude of these unwanted jumps between the neighbouring equilibrium positions can be decreased by a suitable size of the sphere.

1. Introduction

The single-beam optical trap (SBT) has become a routinely used experimental tool in the fields of molecular and cell biology, colloidal chemistry and surface analysis within the past 15 years [1–3]. In the classical trapping scheme, a probe (a dielectric particle) is confined in a tightly focused laser beam [4] and its equilibrium position is, apart from external disturbances, essentially fixed relative to the trapping beam focus. Recently, an alternative to optical trap generation was suggested, which exploits the interference of counter-propagating incident and reflected laser beams in front of a highly reflective slide [5,6]. In this case, the periodically modulated Gaussian standing-wave (GSW) created by superposition of both beams generally contains multiple trapping positions, that is the standing-wave traps (SWTs), which are spatially fixed with respect to the reflective slide. Generation of the oscillating GSW component of the total field, however, is not limited to the surfaces of reflectivity approaching 100% [5]. Thus, in a wide class of experiments, where the SBT is used as a force transducer [7,8] or a tool for fabrication of mesoscopic structures [9] and where one operates in close proximity to a liquid–solid interface, the reflected beam is present and the probe is subject to

Journal of Modern Optics ISSN 0950–0340 print/ISSN 1362–3044 online
http://www.tandf.co.uk/journals
DOI: 10.1080/0950340310000694 51

the combined forces of the SBT and SWTs. Consequently, the response of the probe to the displacements of the SBT obtained by moving the beam focus within the sample can change significantly. Some volume elements can even become inaccessible to SBT manipulation.

The extent to which the reflection from a dielectric interface modifies the SBT manipulation of polystyrene spheres (radius $a = 0.108\,\mu m$) has already been studied theoretically and experimentally [10]. It was demonstrated that, even for an ordinary glass–water interface with a reflectivity as low as $R \approx 0.4\%$, the SWTs dominate the trapping up to 5 μm from the glass surface and affect the trapping to distances several times longer. The region of the dominance of SWTs grows with increasing reflectivity R of the surface and reaches tens of microns for $R = 98\%$. On the other hand, it was shown theoretically that this unwanted grabbing of the probe by SWTs can be suppressed by using a probe with a radius which is a suitable fraction of the trapping wavelength [11]. A sphere of this particular radius is pulled by neighbouring SWTs in opposite directions and, therefore, the resulting SWT axial forces tend to cancel out. We briefly analyse this effect theoretically and demonstrate it experimentally in this article.

2. Theory

2.1. *Optical force calculation*

Theoretical analysis of the interaction between a particle and an electromagnetic wave generally consists of description of the incident beam, the field established owing to the interaction of the incident beam and the particle, and, finally, the forces acting on the particle surrounded by the resulting field. Single-beam optical trapping requires a tightly focused laser beam with a spot diameter comparable with the trapping wavelength. To achieve this, high-quality immersion objectives are usually used. In this case the beam passes through a number of dielectric interfaces (optical elements inside the objective, immersion oil layer, coverslip and water layer) which makes a correct description of the field in the focal region quite complex. The effects caused by diffraction of the beam on the objective back aperture and by spherical aberration due to the refractive index mismatch at the dielectric interfaces below the objective influence strongly the final intensity distribution [12,13]. Despite this fact, the simple Gaussian beam is still the most frequently considered form of the incident beam even though it is only a paraxial solution of the wave equation and it does not treat the polarization components in the focused beam properly. Therefore, to obtain more appropriate formulae for the focused beam, we used a theoretical treatment describing the incident wave as the Gaussian beam corrected to fifth order [14].

Description of the field produced as the result of the interaction of the incident beam and the sphere is a general problem studied by the generalized Lorenz–Mie theory (GLMT) [15,16]. The force interaction between the total outer field and the particle can then be quantified on the basis of the momentum conservation principle (forces acting on any finite volume in a material body can be expressed through the forces applied to the surface of that volume) and on the assumptions that a fluid surrounding the particle is isotropic, non-magnetic, linear in its response to the applied field and in hydrodynamic equilibrium [15,17,18].

Theoretical methods for calculation of the optical forces acting on a sphere placed in a single corrected Gaussian beam (CGB) have been presented indepen-

dently by Ren *et al*. [19] and Schaub *et al*. [15]. For our study we have adapted the approach in [15,20]. We assume that the initial field distribution close to the dielectric interface is created as the interference of the incident CGB and CGB retroreflected from the surface. Because we suppose that the retroreflected beam is only weak, the final axial optical intensity distribution has an incident CGB envelope modulated by a weak standing-wave component with modulation depth proportional to $R^{1/2}$ (R is the surface reflectivity) [5]. Therefore, negligibly low R (a water–glass interface has $R \approx 0.04\%$) can produce a noticeable standing-wave component. If a sphere is inserted into the interference field of the incident and retroreflected CGBs close to a reflective surface, a complex scattering–reflection event occurs [11]. To simplify and speed up the calculation, however, we omit multiply scattered fields between the reflective surface and the sphere. Thus, the incident field distribution that is scattered by the sphere occurs solely by interference of the incident CGB and the counter-propagating reflected CGB. It is thus this distribution which is inserted into the above-mentioned GLMT formalism. To speed up the calculation even more, we assume that the spherical object is located on axis and we can thus employ radial symmetry of the problem [20]. We wrote the modified code for the force evaluation ourselves but we do not present a detailed mathematical description because the method has been well described in the literature [14,15,20].

2.2. *Beam waist approaching the reflective surface*

We want to simulate the behaviour of the trapped sphere while the trapping beam waist approaches the reflective surface. Therefore, we decrease gradually the beam waist distance z_w from the surface, and at each beam waist position we calculate the axial profiles of the intensity $I(z)$ and optical force $F(z)$ acting on the sphere placed within the axial positions $3z_R > z > -z_R$. Here, z is the distance of the sphere centre from the beam waist and z_R is the beam Rayleigh length ($z_R = \pi w_0^2/\lambda$, where w_0 is the beam waist and λ the trapping wavelength in water). We calculate the potential energy of the sphere in the beam as the axial force integral $W(z) = \int_{-\infty}^{z} F(t)\,\mathrm{d}t$. Because the only important parameter of the potential profile is the depth of individual potential wells, we set its minimal value equal to zero. Initially (at the most distant position of the beam waist from the surface) we assume that the sphere is trapped at the equilibrium position which has the deepest potential well. When the waist is moved closer to the surface, we assume that the sphere stays trapped at the current potential well, unless one of the potential barriers surrounding the sphere becomes lower than $10\,kT$ (the generally accepted criterion for the confinement of the particle in the trap). In such a case we assume that the particle escapes over this lowered potential barrier and settles at the neighbouring deeper potential well that is created owing to the interference of incident and reflected waves. If the neighbouring potential well is not deep enough to confine the sphere, the whole process is repeated; the sphere jumps to the nearest deeper trap satisfying the confinement condition. If none of these cases occurs, the particle is released from the trap and settles on the surface. This occurs if the beam waist is very close to the surface or behind it. If the sphere can be trapped, we record its distance from the beam waist as a function of the beam waist position z_w. In the experiments, we monitor the distance of the sphere from the beam waist by measuring the intensity of the two-photon fluorescence (TPF) which is excited in the volume-dyed sphere by the trapping beam. Therefore, we also calculate a quantity that is proportional to the TPF signal at each z_w. This

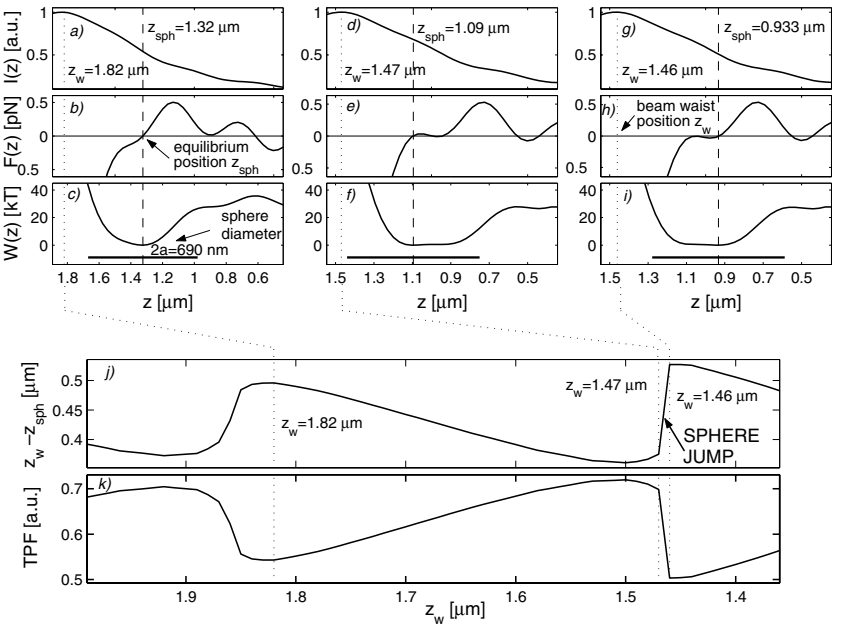

Figure 1. Origin of the trapped probe jumps during approaching of the trapping beam waist to the surface (a.u., arbitrary units). (*a*), (*d*), (*g*) The theoretical profiles of the on-axis intensity $I(z)=|E_x(z)|^2$ (where $E_x(z)$ is the on-axis component of electric field vector), (*b*), (*e*), (*h*) the axial force $F(z)$ and (*c*), (*f*), (*i*) the depth of the potential well $W(z)$ as functions of the sphere–surface distance z at three chosen positions of the beam waist z_w. The trapped sphere is located at z_{sph} (places of zero force and potential minima). The modulations of the envelopes of the single-beam intensity, force and potential are caused by interference of the incident and reflected waves. This means that more than one probe equilibrium position can exist and they could fuse together and create a wider potential well while the beam waist approaches the surface (see (*d*)–(*f*)). Only a 10 nm shift in the beam waist position then causes deformation of the potential well bottom in such a way that the sphere equilibrium position moves by 157 nm (see (*d*)–(*i*)). This change results in a sphere jump of 157 nm further away from the beam waist position (closer to the surface). (*j*) The distance $(z_w - z_{sph})$ between the beam waist and sphere equilibrium positions as a function of the beam waist position. (*k*) Since the trapping beam intensity is different at each equilibrium position, the two-photon fluorescence (TPF) that is excited by the beam in the dyed sphere is another sensitive indicator of the non-uniform sphere motion due to the influence of the reflected wave. The simulation results were obtained for a polystyrene sphere of radius equal to $a=345$ nm (see the thick lines in (*c*), (*f*), and (*i*)), a water–glass interface of reflectivity $R=0.4\%$, a laser power $P=10$ mW, a beam waist size $w_0=0.4\,\mu$m, a sphere refractive index $n_{sph}=1.585$ and a water refractive index $n_{water}=1.332$.

quantity is obtained as the integral of the square of the incident beam intensity over the sphere volume (we assumed at this stage that the intensity inside the sphere is the same as it would be if no sphere were present). The described algorithm together with an illustration of sphere jumps between neighbouring equilibrium positions are schematically shown in figure 1.

It has already been shown [11] that the maximal axial force in the standing-wave trap depends on the sphere size and for certain sphere radii the influence of

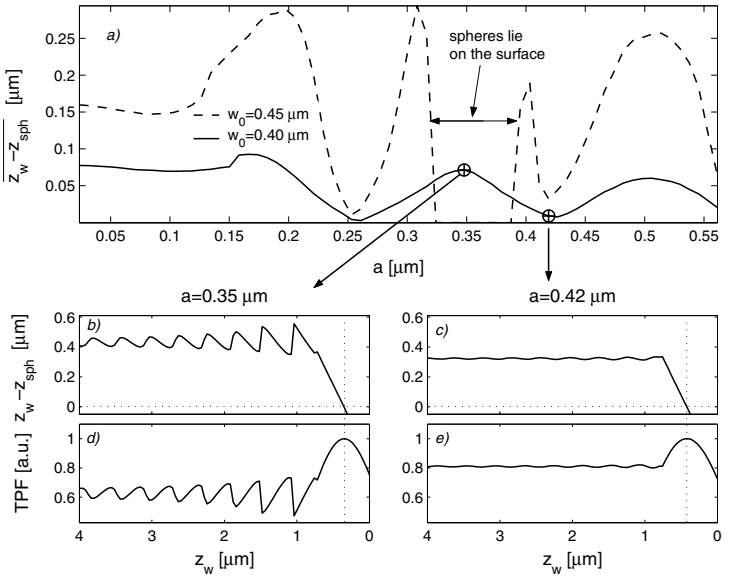

Figure 2. Dependence of the jump length on the polystyrene sphere size. Using the procedure described in figure 1 we analysed behaviour of trapped polystyrene spheres (radii from 30 to 570 nm) as the beam waist approached the surface from a distance of 4 μm. (*a*) The results of this analysis for two beam waist sizes ($w_0 = 0.40\,\mu\text{m}$ and $w_0 = 0.45\,\mu\text{m}$). The quantity $\overline{z_\text{w} - z_\text{sph}}$ is an average value of five subsequent jump lengths starting from the first jump which occurs for $z_\text{w} < 4\,\mu\text{m}$. This procedure provides a smooth curve with visible tendencies of the studied effect. It is seen that a wider beam waist causes longer jumps of the sphere but it is not possible to confine spheres of radii $0.32\,\mu\text{m} < a < 0.38\,\mu\text{m}$. (*a*)–(*e*) We choose two representative sphere radii (one is very sensitive ($a = 0.35\,\mu\text{m}$) and the other is insensitive ($a = 0.42\,\mu\text{m}$) to the standing-wave component) to show (*b*), (*c*) the distance ($z_\text{w} - z_\text{sph}$) of the sphere from the beam waist and (*d*), (*e*) the TPF signal (a.u., arbitrary units) as functions of the beam waist distance from the surface. In these (*b*)–(*e*), the difference in the sphere behaviour is clearly seen together with the fact that the overall maximum of TPF occurs very close to the place where the beam waist position z_w overlaps the sphere centre position z_sph ($z_\text{w} - z_\text{sph} = 0$). We used the following parameters for the simulation: water–glass interface of reflectivity $R = 0.4\%$, laser power $P = 1\,\text{W}$, sphere refractive index $n_\text{sph} = 1.585$ and water refractive index $n_\text{water} = 1.332$.

the standing-wave is completely eliminated. We deduced that a similar effect must exist also at lower surface reflectivities and its existence should decrease the length of the sphere jump between equilibrium positions. Therefore, we proceeded to more extensive simulations and analysed how the length of the sphere jumps depends on the polystyrene particle radius and beam waist size. As shown in figure 2, the length of the jumps can indeed be reduced by appropriate size of the sphere. This jump-suppressing sphere radius also depends on the beam waist size (it slightly decreases with increasing beam waist).

3. Experimental confirmation

3.1. *Experimental procedure*

We wanted to prove experimentally our theoretical conclusions and, therefore, we analysed the behaviour of optically trapped dyed polystyrene spheres as they

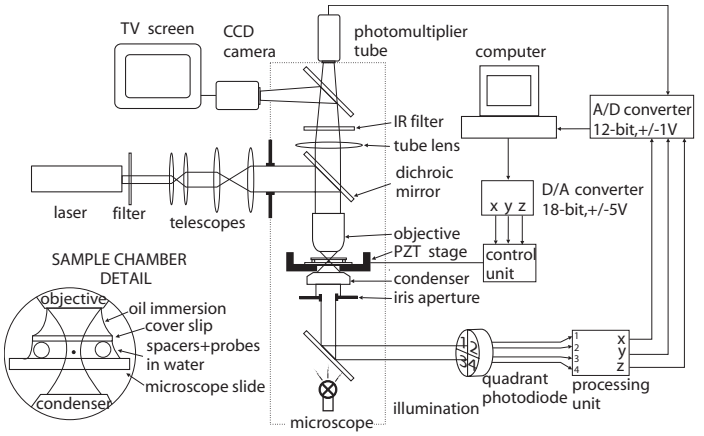

Figure 3. Experimental set-up: TV, television; CCD, charge-coupled device; PZT, piezoelectric transducer; A/D, analogue-to-digital; D/A, digital-to-analogue; IR, infrared. A laser beam emitted by a neodymium-doped YLF laser (Spectra Physics T20-W-105C; $\lambda = 1053$ nm) passes through a filter that blocks the wavelength of the laser-pumping diode light and then it is transformed by a pair of telescopes that enlarge the beam to a diameter of 20 mm. The beam enters the microscope (Olympus, BX 50), reflects from a dichroic mirror (transparent for visible wavelengths) and is finally focused by the microscope objective (Olympus, Ph3 100x OI). The focused beam which has passed through the sample chamber is collimated again by the condenser and then impacts on the quadrant photodiode (EG&G, UV-140BQ-4). The vertical position of the condenser is chosen so that the beam overfills the detector area and condenser numerical aperture is set to 0.5 [21] by an adjustable iris aperture. The TPF from the trapped probe is collected by the objective and detected by a photomultiplier tube (Hamamatsu, R1527). One signal from the photomultiplier tube (PMT) and three from the quadrant photodiode (QPD) are acquired by 12 bit A/D–D/A card (Computer Boards, PCI-DAS4020/12) with a sampling frequency of 60 kHz. The distance between the beam waist and the reflective surface is adjusted by a piezo-stage (Physik Instrumente, PI-517.3C) which is controlled by a (home-made) 18 bit D/A converter via a controlled area network from the computer.

approached a reflective surface. To achieve this, we enhanced the standard experimental apparatus of optical tweezers with two independent particle position detection systems (figure 3). The first detection system employs a PMT to detect weak TPF which is excited in a trapped fluorescent-dyed sphere by the trapping beam. This TPF signal is proportional to the square of the excitation intensity and, therefore, it is very sensitive to the motion of the sphere with respect to the beam waist position but without distinguishing between lateral and longitudinal displacements [22]. Thus, we combined it with the second detection system based on a QPD which was placed behind the condenser to monitor the lateral and longitudinal motions of the sphere from the changes in the intensity pattern [21,23,24].

The sample chamber was formed between a coverslip on the top and a microscope slide, from which the trapping beam was actually reflected, on the bottom (see the detail in figure 3). The space between the two glasses was filled with water that contained suspended probe particles. The thickness of the sample chamber was defined by polystyrene spheres of 9.14 μm diameter (Polysciences, Polybead).

As the probes, we chose two types of red-fluorescent polystyrene microsphere (Duke Scientific; radii, 0.345 and 0.41 μm) that were close to the theoretically predicted jump-enhancing and jump-suppressing radii respectively (see figure 2). The whole sample chamber was sealed with gum adhesive to prevent evaporation. We tested two types of microscope slide: the first with a plain glass surface providing reflectivity in water of $R = 0.4\%$; the second one coated by a system of dielectric TiO_2, and SiO_2 layers of total reflectivity $R = 13\%$. We could, therefore, study the changes in the probe behaviour with respect to the probe radius and reflectivity of the surface.

The change in the distance between the beam waist and microscope slide surface was accomplished by vertical movement of the piezo-driven nanopositioning stage that was operated in a closed-loop regime controlled by the computer. At the beginning of the experiment we trapped a sphere and pushed it against the coverslip surface to the point where the TPF signal emitted from the sphere dropped to approximately 60% of its maximum value. Consequently, the sample chamber was vertically scanned in 20 nm steps so that the probe approached the studied microscope slide on the sample chamber bottom. At each vertical position we waited for 20 ms to stabilize the probe in the new trapping location and then we collected 2048 samples from the QPD and PMT. Mean values and standard deviations of the x, y, z positions of the sphere together with the TPF signals were stored. The chamber scanning was repeated six times (three scans in both directions) to obtain enough data to eliminate the effect of photobleaching of the fluorescent dye on the acquired TPF signals. Such a measurement took typically less than 5 min.

3.2. *Comparison of theoretical and experimental results*

In the theoretical part we defined z_w as the distance between the beam waist and the reflective surface. During the experiment, however, we only know the change Δz_{stg} in the vertical position of the stage. Thus, we must first express z_w in terms of Δz_{stg}. Owing to refractive index mismatch between the coverslip glass and water in the sample chamber, the actual shift Δz_w in the trapping beam waist is scaled with a factor less than 1 with respect to Δz_{stg}. Simple paraxial ray optics considerations can be used to find the relation between the two quantities: $\Delta z_w = (n_{water}/n_{glass})\Delta z_{stg}$ [25]. After insertion of the actual values of refractive indices we obtain $\Delta z_w \approx 0.854 \Delta z_{stg}$.

Secondly, we have to choose a common reference point on the axial axis for both simulation and experiment. We choose the position of the maximum of the TPF signal as this point. A detailed theoretical study revealed that the position of the maximum TPF signal does not precisely coincide with the zero value of $z_w - z_{sph}$. This effect is caused by the presence of the reflected wave and it is more significant for higher surface reflectivity. Therefore, the theoretically found shift was added to the scaled experimental axial positions so that the reference points of theoretical and experimental axis truly overlap.

In the third step we calibrated the QPD axial signal. Here, we employed the part of the experimental QPD curve taken in the proximity of the microscope slide where the sphere was not trapped but, instead, rested on the surface. In this case, the change in distance between the beam waist and the sphere is the same as the change Δz_w in the distance between the beam waist and the surface. One can, thus, use the slope of the dependence of the measured QPD signal on z_w for the QPD

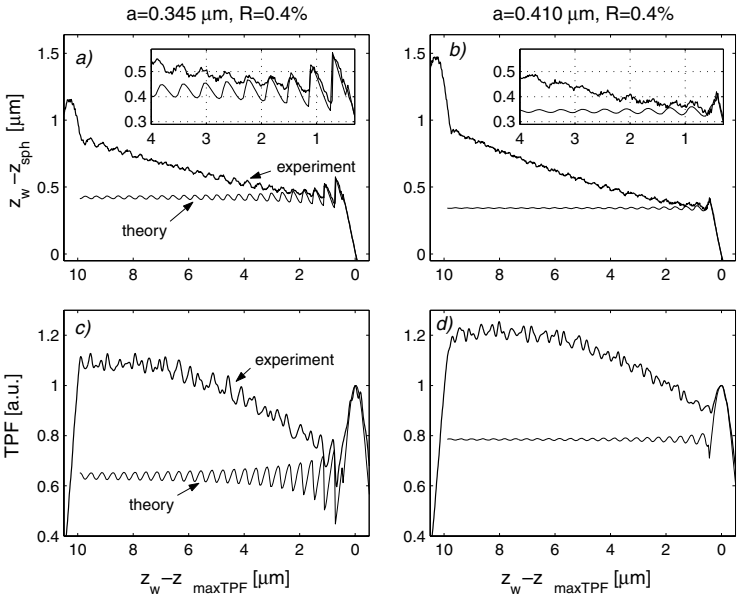

Figure 4. Comparision of theoretical simulation and experimental measurement of the behaviour of polystyrene spheres of radii equal to (*a*), (*c*) $a = 0.345\,\mu\text{m}$ and (*b*), (*d*) $a = 0.410\,\mu\text{m}$ in front of a water–glass interface (reflectivity $R = 0.4\%$). (*a*), (*b*) The distance of the beam waist from the sphere measured by the QPD. The insets show the details of the profiles close to the surface. (*c*), (*d*) The TPF signal measured by the PMT (a.u., arbitrary units). A beam waist size $w_0 = 0.4\,\mu\text{m}$ was considered for both sphere radii.

signal calibration. We calculated this slope over the distance of 200 nm from the zero value of $z_w - z_{sph}$ and divided the measured QPD values by the slope to obtain the shift in the sphere position with respect to the beam waist position in micrometres.

In the fourth step we normalized the theoretical and experimental TPF values to their respective local maxima achieved at the point of contact of the sphere with the reflective surface (position of zero of axial axis).

We calculated the theoretical profiles of TPF and QPD signals for the sphere radii $a = 0.345$ and $0.41\,\mu\text{m}$, sphere and water refractive indices, $n_{sph} = 1.585$ and $n_{water} = 1.332$, and laser power incident on the trapped bead, $P = 50\,\text{mW}$. Reflectivities of the uncoated and coated glass–water interfaces were assumed to be $R = 0.4$ and 13% respectively. The only free parameter, namely the beam waist size w_0, could be in principle obtained from a fit of the expected axial TPF profile shape to the experimental profile of TPF signal for the sphere lying on the surface. Because this peak is not always significant (especially for a larger sphere) and the length of the sphere jumps depends on beam waist size (see figure 2), we calculated instead the theoretical profiles for $w_0 = 0.38$, 0.40 and $0.42\,\mu\text{m}$ and choose that value w_0 which gave better coincidence with the measurement.

The results of both simulations and experiments are summarized in figures 4 and 5 for reflectivities $R = 0.4$ and 13%, respectively. At the beginning of the scans (distance close to $10\,\mu\text{m}$ above the reflective surfaces), the sphere is pressed against the coverslip by moving the trapping beam waist into the coverslip bulk.

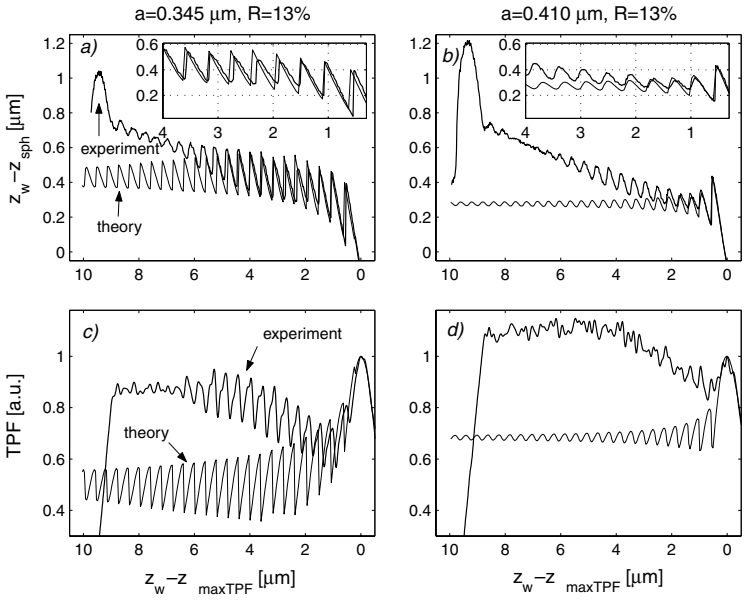

Figure 5. Comparision of theoretical simulation and experimental measurement of the behaviour of polystyrene spheres of radii equal to (*a*), (*c*) $a = 0.345\,\mu m$ and (*b*), (*d*) $a = 0.410\,\mu m$ in front of the water-coated glass interface (reflectivity $R = 13\%$). (*a*), (*b*) The distance of the beam waist from the sphere measured by the QPD. The insets show the details of the profiles close to the surface. (*c*), (*d*) The TPF signal measured by the PMT (a.u., arbitrary units). A beam waist size equal to $w_0 = 0.4\,\mu m$ ($w_0 = 0.38\,\mu m$) was considered for the sphere radius $a = 0.345\,\mu m$ ($a = 0.410\,\mu m$).

Afterwards, the beam waist is moved towards the reflective slide. As the beam waist approaches the sphere, the TPF signal increases until the moment that the sphere is trapped and starts to follow the beam waist motion. The decrease in the TPF signal that occurs afterwards is mainly due to the spherical aberration (caused by the refractive index mismatch between the coverslip and water), which makes the beam waist wider and consequently decreases the on-axis intensity. We also tested the influence of the bleaching of the dye by comparing subsequent records of the TPF signals taken with a known time delay in the same direction. We found, however, that its influence is much smaller than the effect of the spherical aberrations and therefore it was not taken into account. When the beam waist approaches the reflective surface, the QPD signals also decrease. This is due to the increase in the beam width after passing through the condenser lens, which in turn leads to overfilling of the detector. The effects of spherical aberration and overfilling the detector were not considered in the theoretical model used and therefore theoretical TPF and QPD profiles do not decrease as the experimental profiles.

As the beam waist approaches the reflective surface, the intensity modulation due to the GSW component increases and has a stronger influence on the behaviour of the trapped sphere; jumps form a sawtooth-like structure in the profiles. It is clearly seen that these jumps are really caused by the reflection from the surface, since their size generally increases with increasing surface reflectivity. If we compare the position of sphere jumps and their length, we found very good

coincidence between the theory and experiment (see details in figures 4(*a*) and (*b*) and figures 5(*a*) and (*b*)). Moreover, it is seen that the lengths of these measured jumps are indeed much smaller for the larger sphere, which agrees with the conclusions from the theoretical work. More sphere radii should be tested in future to obtain an experimental profile similar to the theoretical profile shown in figure 2(*a*).

4. Conclusion

We demonstrated in this article that the influence of the wave reflected from a dielectric interface on single-beam optical trapping can be suppressed by an appropriate size of the trapped sphere. We tested experimentally polystyrene spheres of radii equal to $a = 0.345$ and $0.410\,\mu\text{m}$ which, according to the theoretical predictions, should be more sensitive and less sensitive, respectively, to the intensity modulation caused by the reflected beam. This effect was indeed observed for two types of reflective interface: water–glass (reflectivity $R = 0.4\%$) and water-coated glass ($R = 13\%$). The agreement between the predicted and measured behaviour of the trapped sphere while the beam waist approached the surface was very good in terms of location and size of discrete jumps of the trapped sphere between neighbouring stable trapping positions.

Acknowledgment

The work was supported by the Grant Agency of the Czech Republic, project 101/00/0974.

References

[1] Greulich, K.-O., 1999, *Micromanipulation by Light in Biology and Medicine* (Basel: Birkhauser).
[2] Masuhara, H., Schryver, F. C. D., Kitamura, N., and Tamai, N., 1994, *Microchemistry, Spectroscopy, and Chemistry in Small Domains* (Amsterdam: North-Holland).
[3] Sheetz, M. P., Wilson, L., and Matsudaira, P., 1998, *Methods in Cell Biology*, Vol. 55, *Laser Tweezers in Cell Biology* (San Diego, California: Academic Press).
[4] Ashkin, A., Dziedzic, J. M., Bjorkholm, J. E., and Chu, S., 1986, *Optics Lett.*, **11,** 288.
[5] Zemánek, P., Jonáš, A., Šrámek, L., and Liška, M., 1998, *Optics Commun.*, **151,** 273.
[6] Zemánek, P., Jonáš, A., Šrámek, L., and Liška, M., 1999, *Optics Lett.*, **24,** 1448.
[7] Sasaki, K., Tsukima, M., and Masuhara, H., 1997, *Appl. Phys. Lett.*, **71,** 37.
[8] Clapp, A. R., Ruta, A. G., and Dickinson, R. B., 1999, *Rev. scient. Instrum.*, **70,** 2627.
[9] Dufresne, E. R., and Grier, D. G., 1998, *Rev. scient. Instrum.*, **69,** 1974.
[10] Jonáš, A., Zemánek, P., and Florin, E.-L., 2001, *Optics Lett.*, **26,** 1466.
[11] Zemánek, P., Jonáš, A., and Liška, M., 2002, *J. opt. Soc. Am.* A, **19,** 1025.
[12] Rohrbach, A., and Stelzer, E. H. K., 2001, *J. opt. Soc. Am.* A, **18,** 839.
[13] Rohrbach, A., and Stelzer, E. H. K., 2002, *Appl. Optics*, **41,** 2494.
[14] Barton, J. P., and Alexander, D. R., 1989, *J. appl. Phys.*, **66,** 2800.
[15] Barton, J. P., Alexander, D. R., and Schaub, S. A., 1989, *J. appl. Phys.*, **66,** 4594.
[16] Gouesbet, G., and Grehan, G., 2000, *Atom Sprays*, **10,** 277.
[17] Robinson, F. N. H., 1975, *Phys. Rep.*, **16,** 313.
[18] de Groot, S. R., and Suttorp, L. G., 1971, *Foundations of Electrodynamics* (Amsterdam: North-Holland).
[19] Ren, K. F., Grehan, G., and Gouesbet, G., 1996, *Appl. Optics*, **35,** 2702.
[20] Schaub, S. A., Barton, J. P., and Alexander, D. R., 1989, *Appl. Phys. Lett.*, **55,** 2709.
[21] Rohrbach, A., and Stelzer, E. H. K., 2002, *J. appl. Phys.*, **91,** 5474.

[22] FLORIN, E.-L., HÖRBER, J. K. H., and STELZER, E. H. K., 1996, *Appl. Phys. Lett.*, **69,** 446.
[23] GITTES, F., and SCHMIDT, C. F., 1998, *Optics Lett.*, **23,** 7.
[24] PRALLE, A., PRUMMER, M., FLORIN, E.-L., STELZER, E. H. K., and HÖRBER, J. K. H., 1999, *Microsc. Res. Technol.*, **44,** 378.
[25] WIERSMA, S. H., and VISSER, T. D., 1996, *J. opt. Soc. Am.* A, **13,** 320.